JACS
JOURNAL OF THE AMERICAN CHEMICAL SOCIETY
Article
pubs.acs.org/JACS

Covalent Capture of Aligned Self-Assembling Nanofibers

I-Che Li and Jeffrey D. Hartgerink*

Departments of Chemistry and Bioengineering, Rice University, 6100 Main Street, Houston, Texas 77005, United States

Supporting Information

ABSTRACT: A great deal of effort has been invested in the design and characterization of systems which spontaneously assemble into nanofibers. These systems are interesting for their fundamental supramolecular chemistry and have also been shown to be promising materials, particularly for biomedical applications. Multidomain peptides are one such assembler, and in previous work we have demonstrated the reversibility of their assembly under mild and easily controlled conditions, along with their utility for time-controlled drug delivery, protein delivery, cell encapsulation, and cell delivery applications. Additionally, their highly compliant criteria for sequence selection allows them to be modified to incorporate protease susceptibility and biological-recognition motifs for cell adhesion and angiogenesis. However, control of their assembly has been limited to the formation of disorganized nanofibers. In this work, we expand our ability to manipulate multidomain-peptide assembly into parallel-aligned fiber bundles. Albeit this alignment is achieved by the shearing forces of syringe delivery, it is also dependent on the amino acid sequence of the multidomain peptide. The incorporation of the amino acid DOPA (3,4-dihydroxyphenylalanine) allows the self-assembled nanofibers to form an anisotropic hydrogel string under modest shear stress. The hydrogel string shows remarkable birefringence, and highly aligned nanofibers are visible in scanning electronic microscopy. Furthermore, the covalent linkage induced by DOPA oxidation allows covalent capture of the aligned nanofiber bundles, enhancing their birefringence and structural integrity.

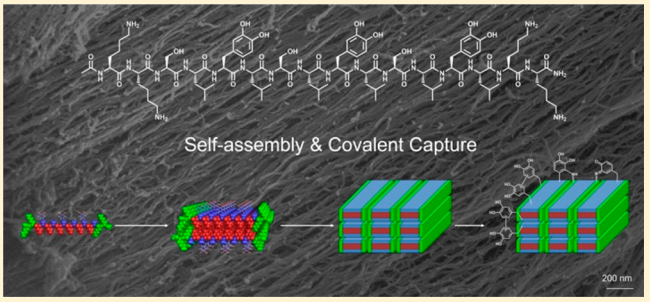

INTRODUCTION

Nature regularly creates highly anisotropic environments, which allows directional movement, aligned application of force, and controlled diffusion. The design of self-assembling systems, particularly "one-dimensional" nanofibers, has advanced considerably in the past decade, and these systems typically self-organize to form a well-structured nanosystem but have little long-range order. In part, this is because of the design of the assembler; it exclusively controls formation of the desired nanofiber but not interfiber interactions. Instead, fiber alignment has relied on more traditional alignment methods, including the use of electric fields,[1,2] liquid crystals,[3,4] and mechanical stretching.[5] However, for biocompatible scaffolds, fabrication of macroscopic alignment is still challenging. Recently, supramolecular chemistry has shown its potential to achieve anisotropic materials.[6] In one case, enzymatic hydrogelation showed that aromatic−aromatic interactions could be used to enhance fibrous alignment.[7] Peptide amphiphiles have also been demonstrated to form aligned monodomain gels via thermally assisted (and other) mechanisms of self-assembly.[8−11] Strategies for other supramolecular biomaterials are still limited.

Multidomain peptides (MDPs) self-assemble into nanofibers with approximately a 6 nm width and they are microns in length. Their self-assembly is based on the ability of hydrophobic packing to stabilize a bilayer structure that is elongated through the formation of a β-sheet hydrogen-bonding network. Their primary sequence can be divided into clearly defined domains: an amphiphilic-core domain composed of alternating hydrophilic−hydrophobic residues and flanking domains comprised of either negatively or positively charged residues.[12] By the addition of salts, the electrostatic repulsion of the charged domains can be quenched, allowing the amphiphilic core to drive nanofiber assembly, and at the appropriate concentration and solvent composition, ultimately generating a three-dimensional hydrogel. In our previous reports, the MDP nanofibers have frequently been observed by electron microscopy and atomic force microscopy to have parallel bundling and short-range alignment.[13−15] MDPs have also been shown to exhibit shear-thinning and shear recovery.[16] Together, this led us to believe that by tuning the balance of aggregation and fiber growth, MDPs would respond to external shearing forces and achieve long-range alignment.

As a result of its biological role, as well as its interesting chemical properties, DOPA (3,4-dihydroxyphenylalanine) has been incorporated into synthetic polymers and biomimetic materials.[17−19] The unique structure of the DOPA side chain allows it to mediate supramolecular interactions, including monodentate and self−self-bidentate hydrogen-bonding, π stacking, and hydrophobic interactions in aqueous systems.[20,21] In addition, DOPA is readily oxidized to *o*-quinone, followed by a variety of cross-linking reactions.[22−25] This oxidation-induced cross-linking pathway is orthogonal to the chemistry

Received: May 6, 2017
Published: June 5, 2017

DOI: 10.1021/jacs.7b04655
J. Am. Chem. Soc. 2017, 139, 8044−8050

used (simple addition of salts) for self-assembly such that one can be triggered without the other.

In this work, we demonstrate a new self-assembly pathway to form long-range aligned MDP nanofibers with the incorporation of DOPA residues. By tuning both the aromatic feature and hydrophilic substitutions of MDPs, peptide aggregation and fiber formation can be balanced to generate a fibrous scaffold with long-range alignment. Both birefringence and SEM evidence demonstrate the successful formation of the aligned nanostructured strings of MDPs. Additionally, we show that the self-assembled nanostructure can be covalently captured by adding oxidants to trigger DOPA cross-linking. Covalent capture makes the material far more robust under a variety of conditions. This assembly pathway provides a new strategy to design biomimetic materials at the nanoscale with long-range order.

RESULTS AND DISCUSSION

Peptide Design and Characterization. A series of MDPs with the general sequence of $K_2(SLXL)_3K_2$ were prepared where X was either serine,[16] phenylalanine, tyrosine, or DOPA (herein abbreviated as Z, the structure is shown in Figure 1).

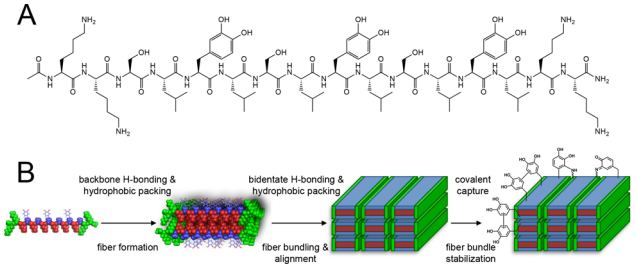

Figure 1. Schematic of multidomain peptides forming aligned self-assembling nanofibers. (A) Chemical structure of DOPA-containing MDP sequence $K_2(SLZL)_3K_2$. (B) Process of self-assembly, fiber bundling, fiber alignment, and covalent capture. The inclusion of DOPA introduces hydrophobic moieties in addition to the potential for bidentate hydrogen bonding on the surface to reinforce the observed parallel packing of fibers. Upon oxidation, these groups can covalently cross-link with one another or with the amines of the lysine residues.

Our hypothesis is that the inclusion of DOPA would introduce hydrophobic interactions on the surface of nanofibers, whereas the hydroxyl groups would help to maintain the fibrous solubility and provide a second mode of interfiber interaction through bidentate hydrogen bonding. The secondary structure and nanostructure were characterized to confirm the peptide self-assembly (Figure 2). FTIR exhibited an amide I parallel peak near 1630 cm^{-1} and an amide I perpendicular peak near 1695 cm^{-1}, which together can be correlated to an antiparallel β-sheet structure. The CD spectrum containing a maximum at 195 nm and a minimum at 216 nm also indicates that the peptide forms a β-sheet structure in aqueous solution. Both techniques revealed that the DOPA substitution does not change the peptide secondary structure significantly from expectations based on the previous MDP assemblies described by us.[12]

Negative-stain transmission electron microscopy (TEM) and scanning electron microscopy (SEM) are shown in Figure 2C and 2D, respectively. In the TEM image of $K_2(SLZL)_3K_2$, the MDP was observed to self-assemble into nanofibers with a similar morphology to the previously reported $K_2(SL)_6K_2$

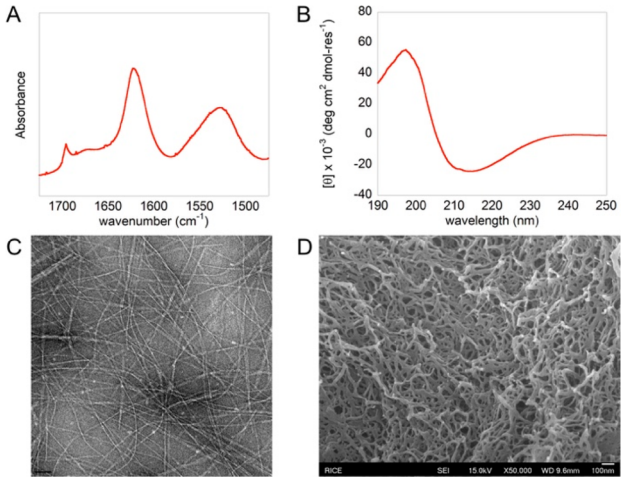

Figure 2. Structural characterization of $K_2(SLZL)_3K_2$. (A) FTIR spectrum showing characteristic peaks for β-sheet: 1630 cm^{-1} and antiparallel: 1695 cm^{-1}. (B) CD spectrum showing characteristic maximums at 195 nm and minimums at 216 nm for β-sheets. (C) Negative-stain TEM and (D) SEM both revealed similar fibrillar structure to the unmodified $K_2(SL)_6K_2$ peptide. Scale bar for C is 50 nm. Scale bar for D is 100 nm.

(Figure S2A). The dimensions of the fibers also remained similar to previously reported MDP nanofibers.[13] To assess the long-range order of the nanofibers, SEM was used. Figure 2D confirmed that the nanofibers were entangled in a random structure, which is consistent with the porous nanofibrous structure of $K_2(SL)_6K_2$ (Figure S2B). The rheological properties (Figure S1B) also behaved similarly to $K_2(SL)_6K_2$. On the basis of the above characterizations, the DOPA-substituted MDP, despite the addition of the aromatic moiety, forms a porous, nanofibrous hydrogel with a similar folding, nanostructure, and long-range alignment.[13]

Long-Range Shear-Induced Alignment. The above characterization was performed on nanofibrous MDP hydrogels which had been prepared by simple mixing of the MDP with HBSS buffer. To examine the possibility of shear alignment of these nanofibers, $K_2(SLZL)_3K_2$ was prepared in a gel-loading tip and slowly injected into the HBSS buffer solution while dragging the pipet backward. Gelation occurs immediately upon mixing and resulted in the formation of a narrow string of hydrogel which was inches long (Figure 3 A,B). The peptide string showed a unique mechanical strength in that it can be easily lifted by tweezers without breaking. Examination of the string by polarized optical microscopy revealed strong birefringence along the length of the fiber (Figure 3C). This suggests that the self-assembled MDP formed an inches-long anisotropic string.

To observe the organization of the nanofibers inside the string, SEM was performed. As showed in Figure 3D, the string was found to be composed of aligned bundles of nanofibers, completely different from what was observed in our simple mixing experiment. Consistent with the birefringence results, this nanofiber alignment was also found extending along the peptide string. Figure S3 also showed the edge section of the string, which revealed that the alignment also exists in the interior of the fiber. The string was broken by pipet mixing and sonication for TEM sample deposition. Aligned nanofiber bundles were frequently observed on the TEM grids (Figure S4). Together, these results show that with careful injection of

DOI: 10.1021/jacs.7b04655
J. Am. Chem. Soc. 2017, 139, 8044−8050

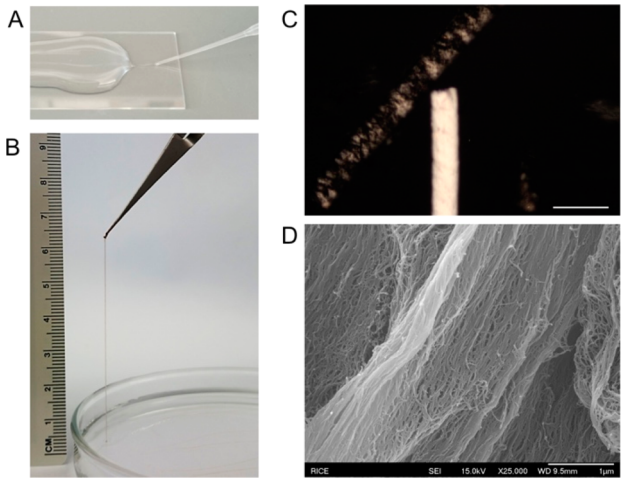

Figure 3. MDP forming strings with macroscopic alignment. (A), (B) $K_2(SLZL)_3K_2$ aqueous solution extrusion into HBSS to form an inches-long peptide string. (C) Birefringence and (D) SEM evidence suggesting uniform alignment along the strings. Scale bar for C is 500 μm. Scale bar for D is 1 μm.

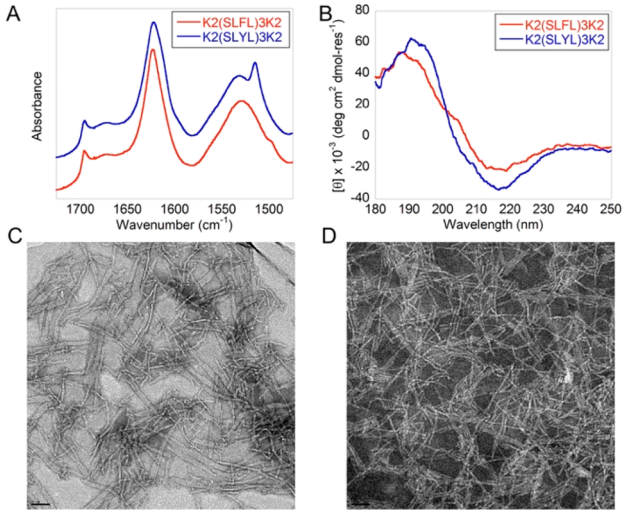

Figure 4. Structural characterization of MDPs $K_2(SLFL)_3K_2$ and $K_2(SLYL)_3K_2$. (A) FTIR spectrum of $K_2(SLFL)_3K_2$ (red) and $K_2(SLYL)_3K_2$ (blue) showing characteristic peaks for an antiparallel β-sheet at 1630 cm^{-1} and 1695 cm^{-1}. The peak at 1517 cm^{-1} is correlated to tyrosine ring C−C stretching and C−H in plane bending. (B) CD spectrum of $K_2(SLFL)_3K_2$ (red) and $K_2(SLYL)_3K_2$ (blue) showing similar characteristic peaks for β-sheet (minimum near 216 nm). (C) TEM of $K_2(SLFL)_3K_2$ revealing short parallel bundles of fibers. (D) TEM of $K_2(SLYL)_3K_2$ showing fewer bundles but increased physical entanglement. Scale bars for (C) and (D) are 50 nm.

the MDP into the appropriate buffer solutions creates long strings of aligned MDP nanofiber bundles.

In order to evaluate the role of DOPA, $K_2(SL)_6K_2$ peptide strings were also made in the same manner. However, $K_2(SL)_6K_2$ strings displayed no birefringence (Figure S2, C and D), which suggested that there is no internal alignment. Additionally, the formed string had poor mechanical strength and easily fractured. Considering the structural difference between $K_2(SL)_6K_2$ and $K_2(SLZL)_3K_2$, the aromatic side chain of DOPA may be playing a key role in the differences in long-range organization. Two additional MDPs were prepared to help elucidate this difference in alignment.

$K_2(SLFL)_3K_2$ and $K_2(SLYL)_3K_2$. In the investigation of long-range alignment formation, $K_2(SLFL)_3K_2$ and $K_2(SLYL)_3K_2$ were synthesized. This allows us to examine MDPs with only small differences in side chain chemistry: phenylalanine with a benzyl ring but no hydroxylation, tyrosine with one hydroxyl group, and DOPA with two. The peptides were dissolved in water to make 2.0 wt % solutions. When we injected the MDP solutions into HBSS buffer as described above, strings were formed in both cases but did not show birefringence, which was similar to $K_2(SL)_6K_2$ (Figure S6). Also, these peptide's strings were not strong enough to be lifted from solution or otherwise manipulated after creation. Instead, the hydrogel strings easily fragmented.

The peptides were characterized by FTIR, CD, TEM, and rheology. In FTIR and CD characterizations, they showed similar spectra to those of $K_2(SLZL)_3K_2$ (Figure 4A,B. The results revealed that both peptides containing aromatic substitutions still self-assemble into an antiparallel β-sheet structure. However, when we added HBSS buffer to the phenylalanine- or tyrosine-containing MDP solutions, both became cloudy and started precipitating. This was unlike $K_2(SLZL)_3K_2$, which formed a clear hydrogel. Examination of the MDP suspension by TEM revealed that their nanostructures have a morphology different from $K_2(SLZL)_3K_2$. As shown in Figure 4C, $K_2(SLFL)_3K_2$ formed fibers which appear shorter and more rigid. Additionally, we frequently observe this MDP forming small bundles composed of two to four fibers running in parallel. $K_2(SLYL)_3K_2$ assembled into longer, more flexible-looking nanofibers in which parallel bundles are not as frequently observed. Additionally, these nanofibers displayed increased physical entanglement as compared to $K_2(SLFL)_3K_2$ (Figure 4D). In rheological characterization (Figure S5, C and D), $K_2(SLFL)_3K_2$ showed a poor G' value of 45 Pa while $K_2(SLYL)_3K_2$ had a high G' value of 537 Pa. This supports our qualitative TEM observation that $K_2(SLYL)_3K_2$ had more physical entanglement.

Contrastively, $K_2(SLZL)_3K_2$ forms much longer nanofibers because, in part, of the improved solvation of the increased hydroxylation of the DOPA side chain. In cast hydrogels, these fibers are kinetically trapped by physical entanglement and are rarely observed to bundle (Figure 2C). However, upon extrusion into the HBSS buffer through a narrow bore needle, fibers are forced into parallel alignment. Once aligned, this arrangement persists, potentially stabilized through the unique bidentate hydrogen bonding known to occur between DOPA residues.[21]

DOPA Oxidation and Covalent Capture. To evaluate the effect of oxidation on long-range alignment, we used sodium periodate, a commonly used chemical oxidant for DOPA.[26,27] Ortho-quinone, the periodate-oxidized product of DOPA, has been reported to cross-link with a variety of amino acids, such as lysine, histidine, and cysteine.[25] The UV−vis spectra of $K_2(SLZL)_3K_2$ treated with sodium periodate were monitored over 24 h (Figure 6A). Before the addition of sodium periodate, the solution only displayed a λ_{max} at 280 nm, which represents the absorption of DOPA.[27,28] After 10 min of periodate addition, two shoulder peaks at 305 and 400 nm appeared. The two peaks match the expected λ_{max} values of DOPA-quinone, revealing the quick oxidation of DOPA. After 24 h, the spectrum shows two broad peaks from 270 to 300 nm and from 490 to 520 nm, which can be assigned to a mixture of the Michael addition product with lysine and di-DOPA products.[29,30] DOPA oxidation was also assessed by the rheological

DOI: 10.1021/jacs.7b04655
J. Am. Chem. Soc. 2017, 139, 8044−8050

properties of $K_2(SLZL)_3K_2$ after oxidation and cross-linking. It was found that treatment with 1 equiv of periodate resulted in hydrogels with the highest G', being over 1000 Pa (Figure S7).

To address the cross-linking in molecular level, ^{1}H NMR spectra were acquired to track DOPA oxidation and cross-linking (Figure 5. A,B). Before the addition of sodium periodate, the peaks in the aromatic region (δ 6.58, 6.68, 6.75) indicated that the sample contained only nonoxidized DOPA peptide. Upon the addition of 1 equiv of periodate, ortho-quinone appeared (δ 6.19, 6.39, 7.09) within 10 min. After 1 h, DOPA peaks were not observable, suggesting DOPA was fully converted to ortho-quinone. After 24 h, all quinone peaks disappeared because of the loss of aromatic hydrogens during cross-linking and decreased isotropic tumbling. In agreement with the UV−vis analysis, the NMR result suggests that periodate triggers DOPA oxidation in less than 10 min and the conversion to cross-linked structures is completed during the following 24 h. MALDI-TOF spectra (Figure 5C) of the oxidized $K_2(SLSZ)_3K_2$ shows peaks for the monomer through the tetramer and possibly higher oligomers. SDS−PAGE (Figure S8) also suggests a high molecular weight, covalently cross-linked system. Collectively, this evidence indicates that the $K_2(SLZL)_3K_2$ peptide can be oxidized in the presence of periodate and ultimately forms via covalent capture through DOPA cross-linking.

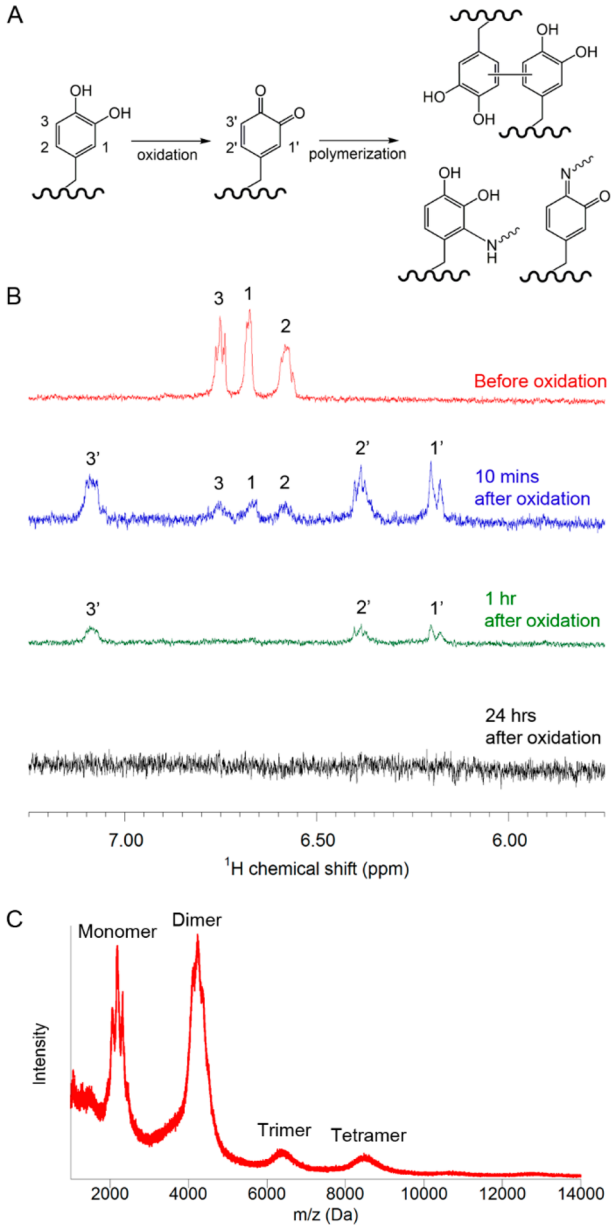

Figure 5. Oxidative cross-linking of $K_2(SLZL)_3K_2$. (A) Scheme showing oxidation of DOPA and possible resulting covalent cross-links. (B) ^{1}H NMR, DOPA, and ortho-quinonone: the protons in the aromatic region are numbered according to the scheme above. Before addition of periodate, aromatic protons are clearly visible. Within 10 min of periodate addition, ortho-quinone is visible, and complete conversion occurs within an hour. After 24 h, the quinone signal disappears, indicating the loss of isotropic tumbling because of polymerization as well as loss of aromatic protons due to cross-linking. (C) MALDI-TOF MS after 24 h of oxidation. Peptide oligomers are observed as evidence for covalent capture.

$K_2(SLZL)_3K_2$ strings were formed in HBSS as before, but this time the HBSS contained 29.3 mM sodium periodate (1 equiv to peptide). Whereas $K_2(SLZL)_3K_2$ self-assembled into aligned nanofiber bundles, DOPA groups are oxidized to DOPA-quinone followed by covalent cross-linking. After 24 h, the strings were examined by polarized microscopy and found to have uniform birefringence (Figure 6C−E). The red color of the strings is related to DOPA-quinone formation and subsequent cross-linking. In the SEM (Figure 6B), it was found that the oxidized DOPA nanofibers formed straight and highly aligned arrays, consistent with the uniform birefringence of the strings.

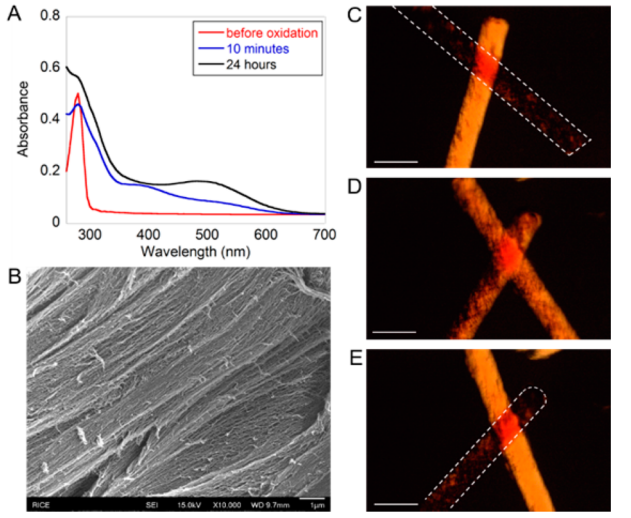

Figure 6. Oxidized $K_2(SLZL)_3K_2$ forming straight and highly aligned arrays with the presence of sodium periodate. (A) UV−vis spectra of $K_2(SLZL)_3K_2$ hydrogel oxidized by sodium periodate in HBSS at pH 7.4. Absorbance was measured before oxidation (red), 10 min (blue), and 24 h (black) after sodium periodate addition. (B) SEM and (C)−(E) birefringence evidence suggesting uniform alignment along the oxidized $K_2(SLZL)_3K_2$ strings. Scale bar for (B) is 1 μm. Scale bars for (C)−(E) are 500 μm.

To analyze the $K_2(SLZL)_3K_2$ string formation process without oxidation, dithiothreitol (DTT) was used to provide a reducing environment.[31] Without DOPA oxidation, the peptide strings still showed birefringence, but it was weaker than it was for the oxidized strings (Figure 7A−C). The SEM also showed that the nanofibers were aligned locally but the bundles were flexible, allowing bends and turns (Figure 7D,E).

DOI: 10.1021/jacs.7b04655
J. Am. Chem. Soc. 2017, 139, 8044−8050

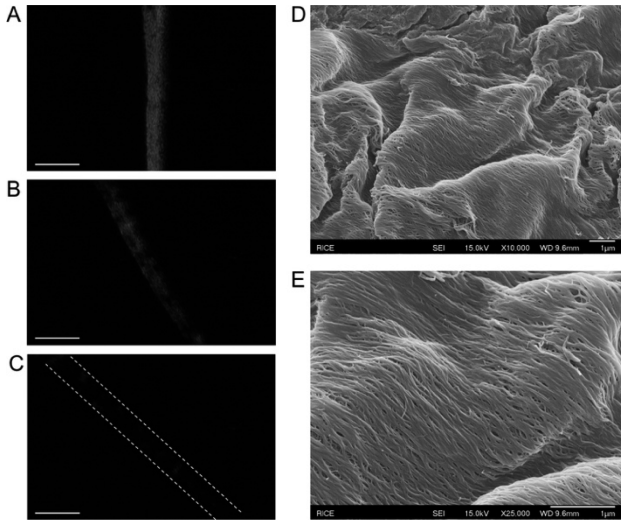

Figure 7. $K_2(SLZL)_3K_2$ forming strings with weak birefringence and wavy bundles with the presence of dithiothreitol (DTT). (A)−(C) Birefringence and (D), (E) SEM evidence suggesting discontinuous orientation of the nanofiber alignment. Scale bars for A−C are 500 μm. Scare bars for D and E are 1 μm.

As a result, the relatively poor orientation of the nanofiber alignment weakened the birefringence of the strings.

We moved both the periodate-treated and DTT-treated strings into deionized water, which removed the phosphate ions required for the ion-bridging that triggers self-assembly. The shape of the strings and their birefringence was monitored to evaluate the integrity of long-range alignment. Before the strings were moved to water, both oxidized strings (Figure 8A)

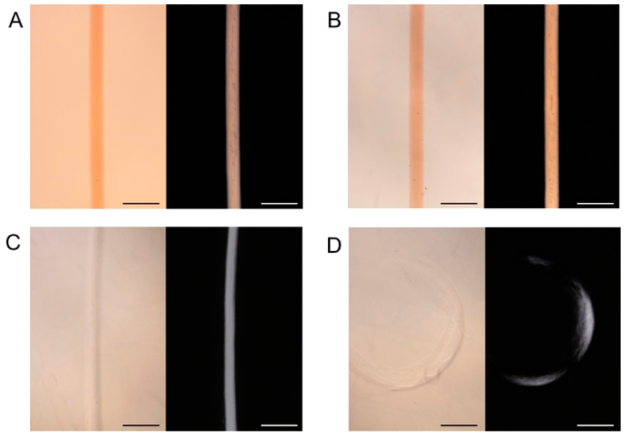

Figure 8. Integrity of shape and birefringence by light microscope. (A) The $K_2(SLZL)_3K_2$ string in $NaIO_4$/HBSS for 24 h and then in (B) water. The string remained straight and birefringent. (C) The string in DTT/HBSS for 24 h was straight and birefringent. (D) After moving to water, the string swelled and fragmented. Bright field (left) and polarized light (right) images were shown. Scale bars: 500 μm.

and nonoxidized strings (Figure 8C) were straight and showed birefringence. After 24 h, the shape and birefringence of the oxidized peptide strings showed no change (Figure 8B), indicating the integrity of the long-range alignment. Without the help of phosphate ions, the covalent cross-links induced by oxidation still bundled the aligned nanofibers, leaving the strings and birefringence unchanged. In contrast, the non-oxidized strings swelled and became fragmented in less than 10 min after being moved to water (Figure 8D). Similarly, the string fragments lost their birefringence, demonstrating that without either ionic or covalent cross-linking the MDP nanofibers and their bundling began to disassemble.

Utilization of DOPA residues in MDPs provides a water-soluble hydrophilic domain to allow self-assembly into nanofibers, yet also contains hydrophobic packing and bidentate hydrogen-bonding characteristics sufficient for stabilizing interfiber interactions that allow these nanofibers to align into parallel bundles upon shearing. DOPA can then be easily oxidized to initiate covalent cross-linking within and between fibers. These covalently captured strings are mechanically strong enough to manipulate and chemically resilient enough to survive transfer into media which, without the covalent cross-links, would result in peptide disassembly. The characteristics of the $K_2(SLZL)_3K_2$ nanofiber strings make them attractive materials for a variety of biomaterial applications.

EXPERIMENTAL METHODS

All chemicals not otherwise specified were purchased from Sigma-Aldrich (Sigma-Aldrich, St. Louis, MO).

Peptide Synthesis. $K_2(SLZL)_3K_2$, $K_2(SLFL)_3K_2$, and $K_2(SLYL)_3K_2$ were synthesized using solid-phase peptide synthesis methodology using a protocol previously reported by us.[13] All resin and coupling reagents were purchased from EMD Chemicals (Philadelphia, PA). After cleavage from the resin, TFA was removed by rotoevaporation. The crude peptides were dialyzed for 3 days using 1000 Da MWCO dialysis tubing (Spectra/Por, Spectrum Laboratories Inc., Rancho Dominguez, CA) against Milli-Q deionized water. $K_2(SLZL)_3K_2$ was dialyzed at pH 3 to help avoid oxidation. The dialyzed peptide solutions were frozen, lyophilized, and then stored at −20 °C. All peptides were characterized by matrix-assisted laser desorption/ionization time-of-flight mass spectrometry, using Autoflex MALDI-TOF MS (Bruker Instruments, Billerica, MA), to verify the correct mass (see Supporting Information).

Circular Dichroism (CD). For CD assessment, the peptide solutions were diluted to 0.01 wt % with water and adjusted to pH 7. The spectra were recorded from 190 to 250 nm with a 0.1 nm data pitch using a Jasco-810 spectropolarimeter (Jasco Inc., Easton, MD). The scan speed was 50 nm/min and the signal was averaged over 5 scans.

Fourier Transform Infrared Spectroscopy (FTIR). Aqueous peptide solutions (0.1 wt %) were adjusted to pH 7 and allowed to dry on the diamond of a "Golden Gate" for attenuated total reflectance (ATR) measurement. The spectra were collected and accumulated from 64 scans on a Jasco FT/IR 660 plus spectrometer (Jasco Inc., Easton, MD).

Transmission Electron Microscopy (TEM). For TEM samples, serial dilutions were performed with Milli-Q water to reach a peptide concentration of 0.01 wt %. The diluted sample solutions were pipetted onto a Quantifoil R1.2/1.3 holey carbon-mesh copper grid and allowed to sit for 1 min. Excess solution was wicked away with filter paper, and the grid was negatively stained with 2 wt % pH 7 phosphotungstic acid (PTA) for 5 min, followed by being dried overnight. Imaging was performed at 100 kV on a JEOL 2010 transmission electron microscope (JEOL USA Inc., Peabody, MA).

Hydrogel Formation. To prepare MDP hydrogels, lyophilized peptides were dissolved to 2 wt % in Milli-Q water, adjusted to pH 7, and subsequently diluted 50:50 with 1× Hank's Buffered Salt Solution (HBSS; Life Technologies), which contains 1.26 mM $CaCl_2$, 5.33 mM KCl, 0.44 mM KH_2PO_4, 0.5 mM $MgCl_2{\cdot}6H_2O$, 0.41 mM $MgSO_4{\cdot}7H_2O$, 138 mM NaCl, 4 mM $NaHCO_3$, 0.3 mM Na_2HPO_4, and 5.6 mM glucose. To prepare the reduced DOPA hydrogel, 2 wt % peptide solution was diluted 50:50 with HBSS containing 293 mM dithiothreitol (DTT) (10 eq. to DOPA concentration). To prepare the oxidized DOPA hydrogel, 2 wt % peptide solution was diluted

DOI: 10.1021/jacs.7b04655
J. Am. Chem. Soc. 2017, 139, 8044−8050

50:50 with HBSS containing 29.3 mM $NaIO_4$ (1 eq. to DOPA concentration). The solution was further diluted to 0.02 wt % for UV−vis absorbance measurement using a TECAN Infinite 200 plate reader (Tecan US, Inc., Morrisville, NC). For MS analysis, 1 eq. $NaIO_4$ was added to prepare the oxidized DOPA hydrogel. After 24 h of oxidation, the hydrogel was dialyzed against Milli-Q deionized water for salt removal. The gel was then homogenized by sonication and further diluted to 0.05 wt %.

Peptide-String Formation. To form peptide strings, the peptides were dissolved to 2 wt % in Milli-Q water. MDP strings were prepared by injecting the 2 wt % peptide solution into HBSS buffer from a Fisherbrand Gel-Loading Tip, 1−200 μL (Thermo Fisher Scientific, Waltham, MA). The tip was dragged backward simultaneously with the injection rate. For the oxidized peptide string, 2 wt % $K_2(SLZL)_3K_2$ aqueous solution was injected into HBSS containing 29.3 mM $NaIO_4$. The peptide string was stored in the oxidizing medium for 24 h to allow the DOPA oxidation to complete. The medium was then replaced by Milli-Q water. For reduced peptide string, 2 wt % $K_2(SLZL)_3K_2$ aqueous solution was injected into HBSS containing 293 mM DTT. The shape and birefringence of the string were subsequently monitored to evaluate the integrity of alignment.

Scanning Electron Microscopy (SEM). In SEM measurement, MDP hydrogels were prepared in the same manner as the hydrogels for TEM. Both MDP strings and hydrogels were dehydrated with a graded ethanol series. Ethanol was then removed from the samples using an EMS 850 critical point dryer (Electron Microscopy Sciences, Hatfield, PA). The dried samples were adhered to SEM pucks with conductive carbon tape and coated with 3 nm of gold using a Denton Desk V Sputter system (Denton Vacuum, Moorestown, NJ). All samples were imaged using a JEOL 6500F scanning electron microscope (JEOL USA Inc., Peabody, MA).

Rheological Analysis. The hydrogels were prepared 24 h before measurement as the protocol described in Hydrogel Formation. The storage modulus (G') and loss modulus (G'') were monitored using a TA Instruments AR-G2 rheometer (TA Instruments, New Castle, DE). Prepared hydrogel was deposited (150 μL) onto the rheometer stage and a 12 mm stainless-steel parallel plate was used with a 1000 μm gap height. In the strain sweep analysis, G' and G'' were monitored under an applied strain of 0.01% to 200% at a frequency of 1 rad/s. In the frequency sweep analysis, G' and G'' were monitored under 1% strain at a frequency of 0.1 rad/s to 100 rad/s. Shear recovery experiments were performed by subjecting the gel to 1% strain for 20 min, increasing the strain to 200% for 1 min, and then reducing the strain back to 1% for 20 min.

Nuclear Magnetic Resonance Spectroscopy (NMR). All peptides were dissolved in D_2O to 0.2 wt % for measurement. The spectra were collected and accumulated from 16 scans on a Bruker AVANCE III HD 600 MHz High Performance Digital NMR (Bruker Instruments, Billerica, MA).

Sodium Dodecyl Sulfate−Polyacrylamide Gel Electrophoresis (SDS−PAGE). For SDS−PAGE separation, all samples were diluted to 0.2 wt %. The DOPA peptide samples were treated with 0.125 equiv, 0.25 equiv, 0.5 equiv, and 1 equiv of periodate, respectively. The samples were then diluted 50:50 with sample buffer containing 4% SDS, 20% glycerol, 10% 2-mercaptoethanol, 0.004% bromphenol blue, and 0.125 M Tris HCl. The final sample loading volume was 10 μL for each well. The samples were then run on a 4−20% gradient gel (4−20%), fixed with 10% glutaraldehyde, and then stained with Coomassie R-250. The imaging was performed on a LAS-4000 Imager (GE Healthcare Bio-Sciences, Pittsburgh, PA).

■ ASSOCIATED CONTENT

Supporting Information

The Supporting Information is available free of charge on the ACS Publications website at DOI: 10.1021/jacs.7b04655.

MALDI-TOF mass spectra, rheological data, TEM and SEM images, SDS-PAGE gel image (PDF)

■ AUTHOR INFORMATION

Corresponding Author

*jdh@rice.edu

ORCID

Jeffrey D. Hartgerink: 0000-0002-3186-5395

Notes

The authors declare the following competing financial interest(s): J.D.H. has stock options in NangioTx, Inc which aims to translate some of the technologies presented in this manuscript towards clinical trials.

■ ACKNOWLEDGMENTS

This work was supported by grants from the Robert A. Welch Foundation (Grant C1557) and from the NIH (R01 DE021798).

■ REFERENCES

(1) Kakade, M. V.; Givens, S.; Gardner, K.; Lee, K. H.; Chase, D. B.; Rabolt, J. F. *J. Am. Chem. Soc.* **2007**, *129*, 2777−2782.

(2) Yoshio, M.; Shoji, Y.; Tochigi, Y.; Nishikawa, Y.; Kato, T. *J. Am. Chem. Soc.* **2009**, *131*, 6763−6767.

(3) Goh, M.; Matsushita, T.; Satake, H.; Kyotani, M.; Akagi, K. *Macromolecules* **2010**, *43*, 5943−5948.

(4) Kang, S. H.; Na, J.-H.; Moon, S. N.; Lee, W. I.; Yoo, P. J.; Lee, S.-D. *Langmuir* **2012**, *28*, 3576−3582.

(5) Matsushita, S.; Akagi, K. *J. Am. Chem. Soc.* **2015**, *137*, 9077−9087.

(6) Webber, M. J.; Appel, E. A.; Meijer, E. W.; Langer, R. *Nat. Mater.* **2016**, *15*, 13−26.

(7) Zhou, J.; Du, X.; Gao, Y.; Shi, J.; Xu, B. *J. Am. Chem. Soc.* **2014**, *136*, 2970−2973.

(8) Zhang, S.; Greenfield, M. A.; Mata, A.; Palmer, L. C.; Bitton, R.; Mantei, J. R.; Aparicio, C.; de la Cruz, M. O.; Stupp, S. I. *Nat. Mater.* **2010**, *9*, 594−601.

(9) Capito, R. M.; Azevedo, H. S.; Velichko, Y. S.; Mata, A.; Stupp, S. I. *Science* **2008**, *319*, 1812−1816.

(10) Cui, H.; Webber, M. J.; Stupp, S. I. *Biopolymers* **2010**, *94*, 1−18.

(11) McClendon, M. T.; Stupp, S. I. *Biomaterials* **2012**, *33*, 5713−5722.

(12) Moore, A. N.; Hartgerink, J. D. *Acc. Chem. Res.* **2017**, *50*, 714−722.

(13) Dong, H.; Paramonov, S. E.; Aulisa, L.; Bakota, E. L.; Hartgerink, J. D. *J. Am. Chem. Soc.* **2007**, *129*, 12468−12472.

(14) Kumar, V. A.; Shi, S.; Wang, B. K.; Li, I. C.; Jalan, A. A.; Sarkar, B.; Wickremasinghe, N. C.; Hartgerink, J. D. *J. Am. Chem. Soc.* **2015**, *137*, 4823−4830.

(15) Li, I.-C.; Moore, A. N.; Hartgerink, J. D. *Biomacromolecules* **2016**, *17*, 2087−2095.

(16) Aulisa, L.; Dong, H.; Hartgerink, J. D. *Biomacromolecules* **2009**, *10*, 2694−2698.

(17) Lee, H.; Dellatore, S. M.; Miller, W. M.; Messersmith, P. B. *Science* **2007**, *318*, 426−430.

(18) Ceylan, H.; Urel, M.; Erkal, T. S.; Tekinay, A. B.; Dana, A.; Guler, M. O. *Adv. Funct. Mater.* **2013**, *23*, 2081−2090.

(19) Kim, B. J.; Oh, D. X.; Kim, S.; Seo, J. H.; Hwang, D. S.; Masic, A.; Han, D. K.; Cha, H. J. *Biomacromolecules* **2014**, *15*, 1579−1585.

(20) Wei, W.; Yu, J.; Broomell, C.; Israelachvili, J. N.; Waite, J. H. *J. Am. Chem. Soc.* **2013**, *135*, 377−383.

(21) Ahn, B. K.; Lee, D. W.; Israelachvili, J. N.; Waite, J. H. *Nat. Mater.* **2014**, *13*, 867−872.

(22) Kutyrev, A. A. *Tetrahedron* **1991**, *47*, 8043−8065.

(23) McDowell, L. M.; Burzio, L. A.; Waite, J. H.; Schaefer, J. *J. Biol. Chem.* **1999**, *274*, 20293−20295.

(24) Yang, J.; Cohen Stuart, M. A.; Kamperman, M. *Chem. Soc. Rev.* **2014**, *43*, 8271−8298.

DOI: 10.1021/jacs.7b04655
J. Am. Chem. Soc. 2017, 139, 8044−8050

(25) Liu, B.; Burdine, L.; Kodadek, T. *J. Am. Chem. Soc.* **2006**, *128*, 15228−15235.
(26) Yu, M.; Deming, T. J. *Macromolecules* **1998**, *31*, 4739−4745.
(27) Burzio, L. A.; Waite, J. H. *Biochemistry* **2000**, *39*, 11147−11153.
(28) Waite, J. H. *Anal. Biochem.* **1976**, *75*, 211−218.
(29) Andersen, S. O.; Jacobsen, J. P.; Bojesen, G.; Roepstorff, P. *Biochim. Biophys. Acta, Protein Struct. Mol. Enzymol.* **1992**, *1118*, 134−138.
(30) Wang, S. X.; Mure, M.; Medzihradszky, K. F.; Burlingame, A. L.; Brown, D. E.; Dooley, D. M.; Smith, A. J.; Kagan, H. M.; Klinman, J. P. *Science* **1996**, *273*, 1078−1084.
(31) Alfonta, L.; Zhang, Z.; Uryu, S.; Loo, J. A.; Schultz, P. G. *J. Am. Chem. Soc.* **2003**, *125*, 14662−14663.

DOI: 10.1021/jacs.7b04655
J. Am. Chem. Soc. 2017, 139, 8044−8050